

MODEL MODIFICATION OF TRANSONIC AERODYNAMIC FORCE ON A HIGH-ASPECT-RATIO AEROELASTIC WING AND ITS ACTIVE FLUTTER

A. Fujimori*, H. Matsushita** and K. Saitoh**

* Department of Mechanical Engineering, Shizuoka University
3-5-1 Johoku, Hamamatsu 432-8561, Japan, a-fujimori@eng.shizuoka.ac.jp

** National Aerospace Laboratory,
6-13-1 Ohsawa, Mitaka, Tokyo 181-0015, Japan

Keywords: *Active flutter suppression, model uncertainty, unsteady aerodynamic force, wind tunnel experiment*

Abstract

This paper presents a model modification of a high-aspect-ratio aeroelastic wing and its active flutter suppression (AFS). One of errors in the linear model of the wing in the transonic region exists in the unsteady aerodynamic force, which is represented by a rational function. To reduce the error, the linear model of is modified in terms of the unsteady aerodynamic force so that the flutter dynamic pressure of the linear model coincides with the one obtained by wind tunnel experiment. Using the modified linear model, AFS controllers are then designed by H_∞ control synthesis and controller reduction. The control performance is evaluated by numerical simulation and wind tunnel experiment.

1 Introduction

Supersonic transport (SST) projects have been a great attention in European countries and USA [1], [2]. Also in Japan, a research project for establishing SST technologies with sub-scaled supersonic experimental aircraft has been promoted by national aerospace laboratory and universities in Japan [3]. The stiffness of SST wings is, in general, low due to reduction of the weight. This low-stiffness deteriorates flutter margins especially in transonic region. Therefore, active flutter suppression (AFS) is one of necessary technologies for the SSTs [4]. Saitoh et al. had reported control syntheses of the AFS in the transonic region using a high-

aspect-ratio aeroelastic wing [5]-[7]. In those studies, the wing was modeled by a linear time invariant (LTI) system and controllers for the AFS were designed. The effectiveness of control performance was evaluated by both numerical simulation and wind tunnel experiments. However, there was a great difference of the control performance; that is, suppressing flutter, between the numerical simulation and the wind tunnel experiment. The reason was that the modeling error might be increased with change of the dynamic pressure. To improve flutter suppression in wind tunnel experiment, it is necessary that the linear model is modified to reduce the error and a robust controller is then designed with the modified model.

One of uncertainties in the linear model of the high-aspect-ratio wing exists in the unsteady aerodynamic force. This paper proposes a model modification of the unsteady aerodynamic force by using an experimental technique. That is, the aerodynamic force in the model is adjusted so that the flutter point of the linear model coincides with the one obtained by wind tunnel experiment. Since the design point for AFS is selected beyond the open-loop flutter point to get a flutter margin, this modification is also done beyond the flutter point. Using the modified model, controllers for the AFS are designed by H_∞ control synthesis and controller reduction. The control performance and the model modification are evaluated by numerical

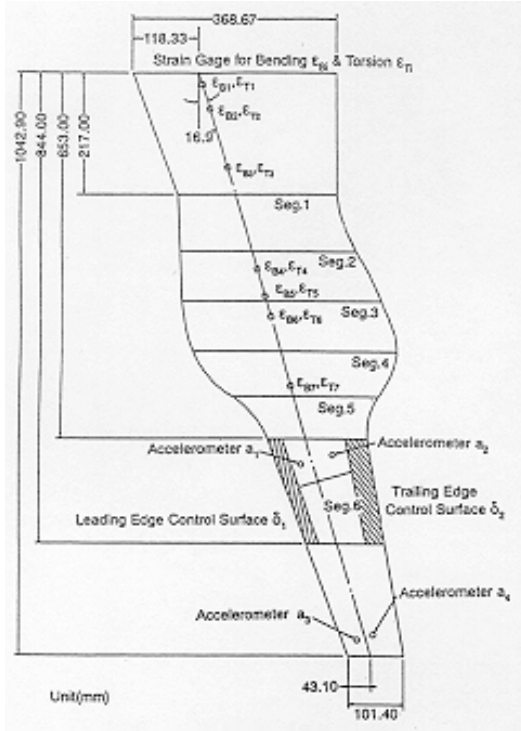


Fig. 1 High-aspect-ratio wing

simulation and wind tunnel experiments.

2 Linear Model of High-Aspect-Ratio Wing

Figure 1 shows a sketch of a high-aspect-ratio aeroelastic wing used in this study. This wing was designed by downsizing a transport-type wing: the span length was 1043 mm, the chord length 369 mm at the root, 101 mm at the tip, and the sweep-back at the quarter-chord 17 deg. The response of the wing was measured using four accelerometers and seven strain gauges as shown in Fig. 1. The wing had leading- and trailing-edge control surfaces δ_1 and δ_2 which were activated independently by two high performance AC servo-motors. Since these motors were contained in the wing, the wing in the middle span was expanded. In this study, only the trailing-edge control surface was used for control and accelerometer a_2 was used as the output in the AFS control design.

Consider N structural modes of the aeroelastic wing. Letting $\xi(t) \in \mathfrak{R}^N$ be the generalized coordinate and $\delta_2 \in \mathfrak{R}^1$ be the

Table 1 Natural frequencies of high-aspect-ratio aeroelastic wing

Mode	Frequency [Hz]
1st	13.1
2nd	35.7
3rd	44.6
4th	85.0

deflection angle of the trailing-edge control surface, the motion of equation of the aeroelastic wing is given by

$$M\ddot{\xi} + D\dot{\xi} + K\xi + S\ddot{\delta}_2 = F(q) \quad (1)$$

where $M, D, K \in \mathfrak{R}^{N \times N}$ are respectively the mass, damping and stiffness matrices associated with the main-wing, and $S \in \mathfrak{R}^{N \times 1}$ is the mass matrix associated with the control surface [5]. $F(q)$ is the unsteady aerodynamic force and is a function of the dynamic pressure q . In this study, four structural modes were taken into account for modeling; that is, $N = 4$. Table 1 shows the natural frequencies of these structural modes.

To derive a linear model of the wing, $F(q)$ is modeled by a linear rational function

$$F(q) = A_{2\xi}\ddot{\xi} + A_{2\delta}\ddot{\delta}_2 + \sqrt{q}A_{1\xi}\dot{\xi} + \sqrt{q}A_{1\delta}\dot{\delta}_2 + qA_{0\xi}\xi + qA_{0\delta}\delta_2 + r \quad (2)$$

$$\dot{r} = \Lambda r + q^{3/2}B_{0\xi}\xi + q^{3/2}B_{0\delta}\delta_2 \quad (3)$$

to approximate the pressure distribution on the aeroelastic wing obtained by the doublet point method (DPM) [8]. $A_{i\xi}, A_{i\delta}$ ($i = 0, 1, 2$), $B_{0\xi}$ and $B_{0\delta}$ are the aerodynamic matrices and $r(t) \in \mathfrak{R}^N$ is an auxiliary variable which represents memory of the unsteady aerodynamic force. $\Lambda \in \mathfrak{R}^{N \times N}$ is a diagonal matrix whose elements are time constant of r_i ($i = 1, \dots, N$).

The equation of the control surface is given as a second-order system

$$\ddot{\delta}_2 + 2\zeta\omega_n\dot{\delta}_2 + \omega_n^2\delta_2 = \omega_n^2\delta_c + w \quad (4)$$

where ω_n is the natural frequency of the actuator, ζ the damping coefficient, δ_c the command and w a white noise included in the actuator. According to the frequency response of the actuator, ω_n and ζ were obtained as $\omega_n = 314$ rad/s and $\zeta = 0.7$. Since a digital computer was used for calculating control law in wind tunnel experiments, an anti-aliasing filter for noise reduction of accelerometer and an analog-digital (A/D) converter were needed. Then, their transfer functions are respectively given as first-order systems

$$G_f(s) = \frac{\omega_f}{s + \omega_f} \quad (5)$$

$$G_d(s) = \frac{s - \omega_d}{s + \omega_d} \quad (6)$$

The cut-off frequency of $G_f(s)$ was given as $\omega_f = 471$ rad/s (=75 Hz) to reduce the resonance of the fourth structural mode of the wing. While that of $G_d(s)$ was given as $\omega_d = 6283$ rad/s (=1000 Hz) because the sampling time of the digital computer was 500 Hz.

Combining Eqs. (1) - (6), a linear model of the high-aspect-ratio aeroelastic wing is given by a linear parameter varying (LPV) system

$$\begin{cases} \dot{x} = A(q)x + B(q)u + B_n w \\ y = C(q)x + D(q) + v \end{cases} \quad (7)$$

$$x \equiv [\xi^T \quad \delta \quad \dot{\xi}^T \quad \dot{\delta} \quad r^T \quad \eta^T]^T$$

$$u \equiv \delta_c \in \mathfrak{R}^1 \quad y \equiv a_2 \in \mathfrak{R}^1$$

where $\eta(t) \in \mathfrak{R}^2$ is a state vector for $G_f(s)$ and $G_d(s)$, and $v(t)$ is a white noise included in the accelerometer. The details of derivation is referred to [5].

3 Model Modification

This section describes a model modification of the LPV system Eq. (7). First, the modified

coefficients of the aerodynamic matrices are introduced. A wind tunnel experiment to decide the modified coefficients is next explained.

3.1 Modified coefficient

In the previous works by Saitoh [5]-[7], the aerodynamic matrices in Eqs. (2) and (3) were regarded as constant with respect to the dynamic pressure q . However, Eq. (2) is a representation to approximate the unsteady aerodynamic force obtained by the DPM with a linear rational function. Furthermore, since the DPM is generally used for subsonic region, it is not claimed that the unsteady aerodynamic force in the transonic region is correctly obtained by the DPM. This paper modifies the aerodynamic matrices as follows:

$$\tilde{A}_{i\xi} = A_{i\xi} r_f(q), \quad \tilde{A}_{i\delta} = A_{i\delta} r_f(q) r_s(q) \quad (8)$$

$$(i = 0,1,2)$$

$$\tilde{B}_{0\xi} = B_{0\xi} r_f(q), \quad \tilde{B}_{0\delta} = B_{0\delta} r_f(q) r_s(q) \quad (9)$$

where $r_f(q)$ and $r_s(q)$ are the modified coefficients and depend on the dynamic pressure q . The coefficients are then adjusted so that the flutter point of the linear model coincides with that of the experimental result. The following cases are assumed on the modified coefficients.

Case-a: The aerodynamic matrices of the main-wing are constant, while those of the control surface depend on q .

$$r_f = r_{f0} (= const), \quad r_s = r_s(q) \quad (10)$$

Case-b: All the aerodynamic matrices depend on q .

$$r_f = r_f(q), \quad r_s = 1 \quad (11)$$

Case-c: The aerodynamic matrices of the main-wing depend on q , while those of the control surface are constant.

$$r_f = r_f(q), \quad r_s = \frac{r_{f0}}{r_f(q)} \quad (12)$$



Fig. 2 High-aspect-ratio wing in transonic wind tunnel

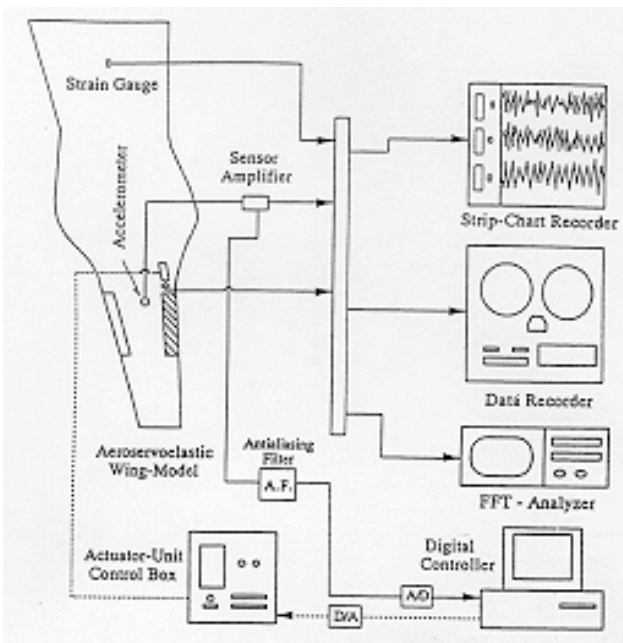


Fig. 3 Experiment system for AFS

3.2 Decision of modified coefficients

The procedure which $r_f(q)$ and $r_s(q)$ are decided by wind tunnel experiment is given as follows:

Step 1: Select a design point $q = q_d$ which is greater than the open-loop flutter dynamic

pressure q_{f0} and design a stabilizing controller $K(s)$.

Step 2: Perform wind tunnel experiments using the designed controller $K(s)$ and record the flutter dynamic pressure, where the output gain of $K(s)$ is changed as follows:

$$K_c = 0.25, 0.50, 0.75, 1.00 \quad (13)$$

Step 3: Construct the closed-loop system which combines the LPV plant Eq. (7) with the controller $K_c K(s)$. Then, $r_f(q)$ and $r_s(q)$ are adjusted so that the flutter dynamic pressure of the closed-loop system coincides with that of the experimental result.

After repeating the above procedure for multiple controllers, the three cases for $r_f(q)$ and $r_s(q)$ are evaluated.

3.3 Wind tunnel experiment for modified coefficients

Figure 2 shows a photo of the high-aspect-ratio aeroelastic wing which was attached at the ceiling in a transonic wind tunnel. Figure 3 shows a sketch of the experiment system. The signal of the accelerometer a_2 was fed to a digital computer through an anti-aliasing filter and an A/D converter. The control law which was derived by digitalizing $K_c K(s)$ was calculated in the computer and the actuator command $u = \delta_c$ was put out to the actuator unit control box through a digital-analog (D/A) converter. The sampling period of the above procedure was 500 Hz. The output signals were recorded by a data recorder and were displayed at a strip-chart recorder and a FFT analyzer.

The experiment condition was given as follows: Mach number was fixed at 0.8 and the dynamic pressure q was changed from 23 to 29 kPa to provide an environment which flutter occurred. At this experiment, the open-loop flutter dynamic pressure was $q_{f0} = 25.40$ kPa.

Figures 4-7 show the plots of the modified

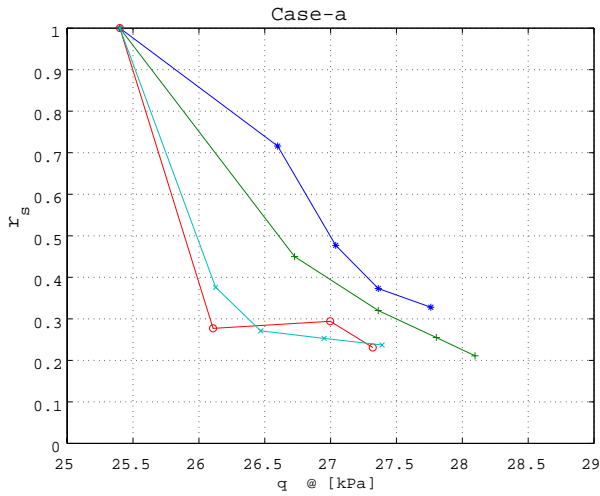


Fig. 4 Modified coefficient $r_s(q)$ Case-a

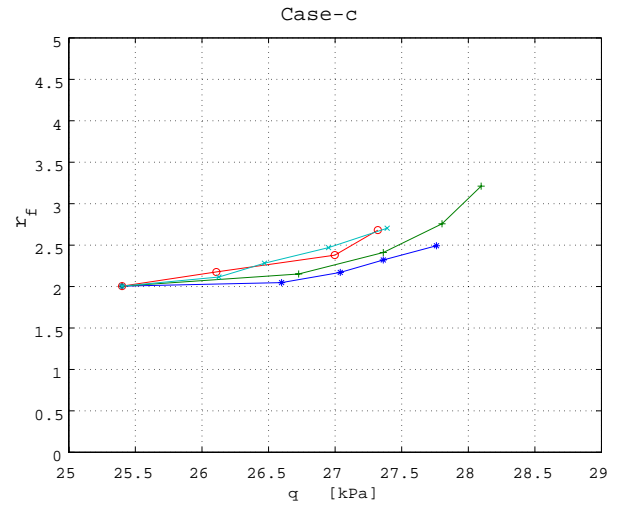


Fig. 6 Modified coefficient $r_f(q)$ Case-c

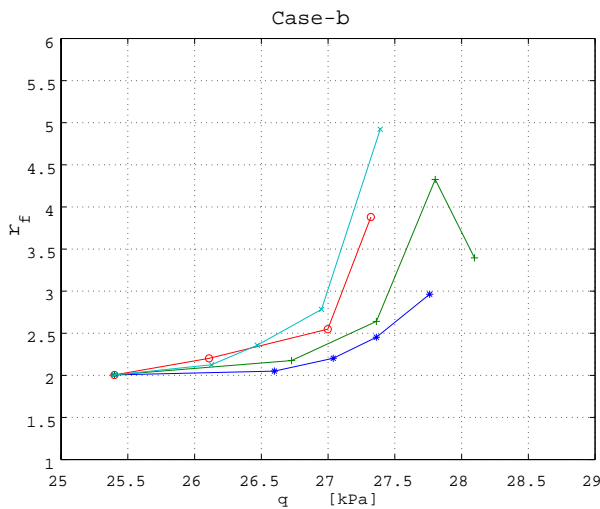


Fig. 5 Modified coefficient $r_f(q)$ Case-b

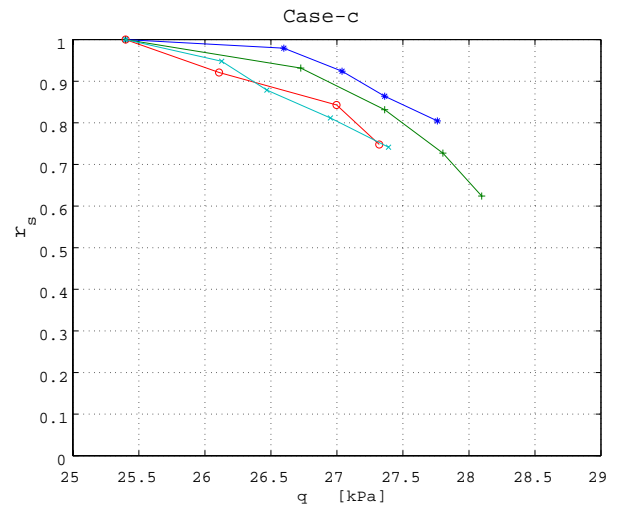


Fig. 7 Modified coefficient $r_s(q)$ Case-c

coefficients $r_f(q)$ and $r_s(q)$ with respect to the dynamic pressure q . Since four controllers were applied, the lines shown in these figures were obtained by changing the output gain K_c as Eq. (13). Evaluating the three adjusting cases, Case-c was the most invariant with respect to the controllers applied. Therefore, Case-c was adopted for modification of the linear model of the wing in this paper. Applying the least square method to Fig. 6, an approximate function of $r_f(q)$ was obtained as

$$r_f(q) = 1.1509 \times 10^{-4} q^3 + 3.002 \times 10^{-2} \quad (14)$$

$r_s(q)$ was given by substituting Eq. (14) into Eq. (12).

4 Active Flutter Suppression (AFS)

Controllers for the AFS were re-designed using the modified LPV plant model Eq. (7) with $r_f(q)$ and $r_s(q)$. The model modification and the control performance was evaluated by wind tunnel experiment.

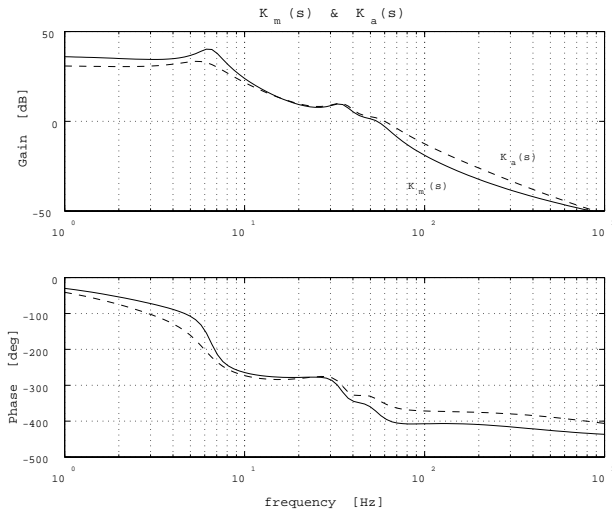


Fig. 8 Frequency response of controllers K_m and K_a

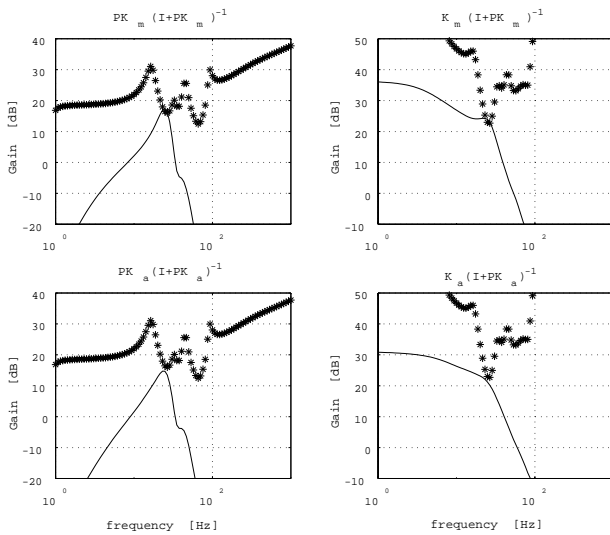


Fig. 9 Complementary and quasi-complementary sensitivity function

4.1 Controller design

Controllers for the AFS were designed in the frame of the robust stabilization in H_∞ control synthesis. Let $P(s)$ and $\tilde{P}(s)$ be a designed plant with $q = q_d$ and a perturbed plant with $q = q_e$ ($q_e > q_d$), respectively. $\tilde{P}(s)$ is then expressed as

$$\tilde{P}(s) = (1 + \Delta_m(s))P(s) \quad (15)$$

$$= P(s) + \Delta_a(s) \quad (16)$$

where $\Delta_m(s)$ and $\Delta_a(s)$ were respectively the multiplicative and the additive uncertainties and are bounded by rational functions $W_m(s)$ and $W_a(s)$ as

$$|\Delta_m(j\omega)| < |W_m(j\omega)|, \quad \forall \omega \quad (17)$$

$$|\Delta_a(j\omega)| < |W_a(j\omega)|, \quad \forall \omega \quad (18)$$

Then, controllers are designed so as to stabilize the closed-loop system and satisfy the following H_∞ norm constraints [9]:

$$\|W_m PK(I + PK)^{-1}\|_\infty < \gamma \quad (19)$$

$$\|W_a K(I + PK)^{-1}\|_\infty < \gamma \quad (20)$$

where γ is a positive bound. Since Eq. (7) was a 16th-order system and $W_m(s)$ or $W_a(s)$ was added to the generalized plant in H_∞ control synthesis [9], the order of H_∞ controllers was too high to perform the digital computer with the sampling period of 500 Hz. The order of the controllers was then reduced to eight by the extended coprime factorization (weighted) (ECFW) controller reduction method [10].

4.2 Frequency response of controller

Figure 8 shows the frequency responses of the designed controllers, where the design point was selected at $q_d = 1.15q_{f0}$. The controller satisfying Eq. (17) is denoted as K_m , while the one satisfying Eq. (18) is as K_a . There was a difference of the gain property between K_m and K_a in the region of 60 - 300 Hz. To evaluate the robust stability, Fig. 9 shows the complementary sensitivity function $T \equiv PK(I + PK)^{-1}$ and the quasi-complementary sensitivity function $T_a \equiv K(I + PK)^{-1}$. The line denoted “*”

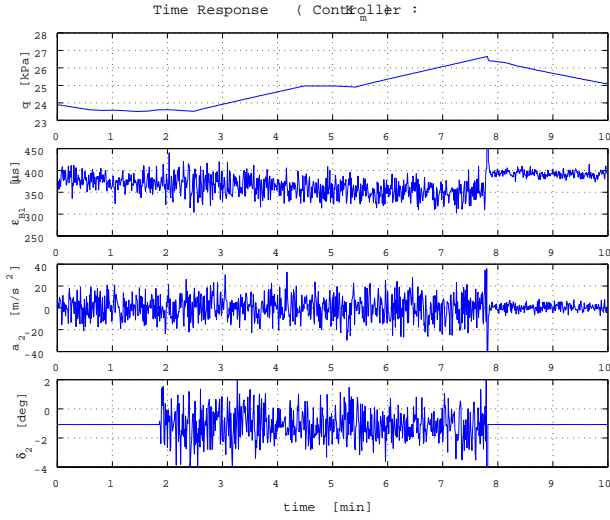


Fig. 10 Time history in AFS experiment, Controller: K_m

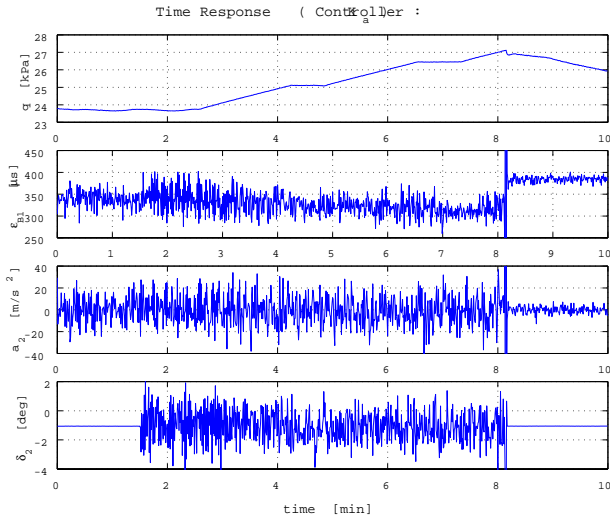


Fig. 11 Time history in AFS experiment, Controller: K_a

indicates the upper bound of the robust stability; that is, the right hand-side of the following inequalities

$$\bar{\sigma}[T(j\omega)] < 1/\bar{\sigma}[\Delta_m(j\omega)] \quad \forall \omega \quad (21)$$

$$\bar{\sigma}[T_a(j\omega)] < 1/\bar{\sigma}[\Delta_a(j\omega)] \quad \forall \omega \quad (22)$$

where $q_e = 1.25q_{f0}$. Comparing the frequency responses, K_a is more robust than K_m .

Table 2 rms* values in AFS control experiments, controller: K_m

Time period (min)	ε_{B1} (μs)	a_2 (m/s^2)	δ_2 (deg)
Term-1 (1.5)	14.625	9.532	0
Term-2 (2.2)	22.977	10.194	1.4750
Term-3 (4.5)	16.614	10.162	0.9334
Term-4 (7.5)	21.550	12.493	1.0960

* rms values were calculated by using data during 10 sec at the beginning of time written in the brackets.

Table 3 rms* values in AFS control experiments, controller: K_a

Time period (min)	ε_{B1} (μs)	a_2 (m/s^2)	δ_2 (deg)
Term-1 (1.0)	17.643	10.721	0
Term-2 (1.7)	30.138	12.658	1.4913
Term-3 (4.4)	19.044	10.753	0.9265
Term-4 (7.9)	23.599	13.402	1.1721

* rms values were calculated by using data during 10 sec at the beginning of time written in the brackets.

4.3 AFS experiment

The designed controllers were evaluated by wind tunnel experiments. The experiment condition was the same as that in Section 3.3. Figures 10 and 11 show the time histories of the dynamic pressure q , the bending strain at the wing-root ε_{B1} , the acceleration a_2 and the deflection angle of the control surface δ_2 . Since the open-loop flutter dynamic pressure was $q_{f0} = 24.10$ kPa in this wind tunnel experiment, the flutter control was turned on below $q = 24$ kPa and q was increased to flutter. In Fig. 11 in which K_a was applied, the amplitude of ε_{B1} and a_2 during $t=1.5 - 3$ min (control-on) was increased rather than that $t=0 - 2$ min (control-off). The amplitude during $t=4 - 6$ min was however reduced where the dynamic pressure was about $q = 25.1$ kPa. Since the design point of AFS controllers was selected at $q_d = 1.15q_{f0}$,

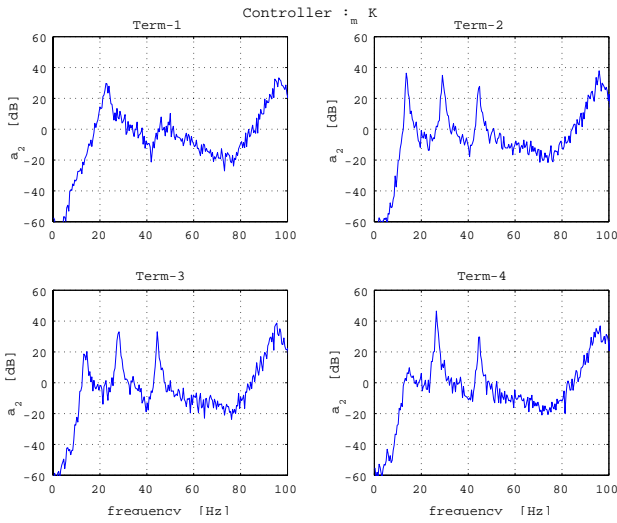


Fig. 12 PSD, Controller: K_m

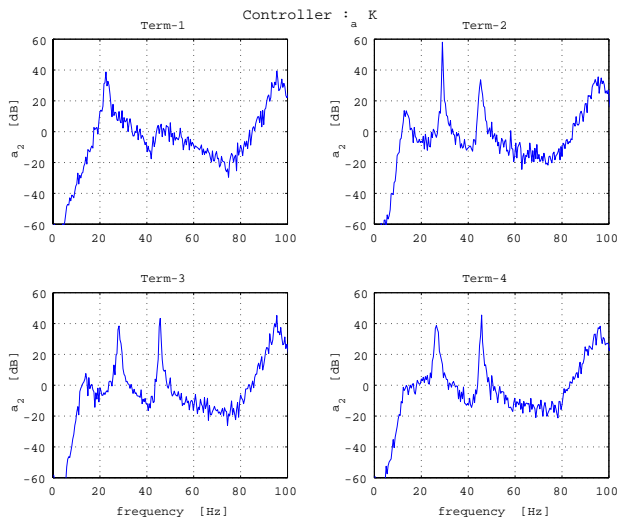


Fig. 13 PSD, Controller: K_a

the model error during $t=4 - 6$ min ($q > q_{f0}$) was smaller than that during $t=1.5 - 3$ min ($q < q_{f0}$). At $t=8.15$ min, flutter suddenly occurred and the flutter stopper stood to reduce the dynamic pressure immediately. Figure 10 shows similar responses.

Figures 12 and 13 show the power spectral density (PSD) corresponding to the time periods shown in Tables 2 and 3. In Term-1 (control-off), the first and the second structural modes are close to each other. The two modes began to couple and a peak was growing at 22.6 Hz

Table 4 Flutter dynamic pressure obtained in numerical simulation and wind tunnel experiment

Controller	Model		Experiment
	Original	Modified	
K_m	34.80 (37%)*	30.48 (20%)	26.77 (9.6%)
K_a	37.85 (49%)	31 (22%)	27.10 (12.1%)

* The values in brackets indicate increased ratio of flutter dynamic pressure.

which was the flutter frequency. In Term-2 which control had just been turned on, the two structural modes were separated by activating the trailing-edge control surface. Since the peaks of the two modes were still large, the amplitude of the time histories was not reduced. In Term-3, the peaks was reduced rather than those in Term-2. In Term-4, the first and the second structural modes were again approached.

5 Evaluation of Model Modification and Control Performance

Table 4 summarizes the flutter dynamic pressure using controllers K_m and K_a in numerical simulation and wind tunnel experiments. Although the proposed model modification was a little effective in estimating the flutter dynamic pressure, there was still a large difference between the numerical and the experimental results. In this study, there were problems in the wind tunnel experiments for the AFS. It was hard to maintain the same experimental condition every time. The temperature inside the wind tunnel was increased during the experiments by 2 - 4 K. Repeating the flutter experiments, the open-loop flutter dynamic pressure was decreased. This may result from decreasing the stiffness of the aeroelastic wing.

Another problem was that the amplitude of the control surface should be taken into consideration. The actuator used in the experiments had a nonlinearity associated with the amplitude. Increasing the amplitude of the deflection angle, the bandwidth of the actuator

was decreased. The model uncertainty in the actuator became larger. Consequently, the control performance was decreased. Therefore, the AFS controllers should not require large amplitude of the control surface.

6 Concluding Remarks

This paper has presented a model modification of a high-aspect-ratio aeroelastic wing and active flutter suppression (AFS). To reduce the uncertainty, the linear model of the wing was modified in terms of the unsteady aerodynamic force so that the flutter pressure of the linear model coincided with the one obtained by wind tunnel experiment. Using the modified linear model, AFS controllers were then designed by H_∞ control synthesis and controller reduction. The control performance was evaluated by numerical simulation and wind tunnel experiments.

There was still a large difference between the numerical and the experimental results. To reduce the difference and improve the flutter suppression effect, controllers should be designed by taking into consideration the input bound.

References

- [1] Quinton, P. P., "Future SSTs: A European Approach," *Aerospace America*, Sept., 1994, pp. 38-43.
- [2] Wilhite, A. W. and Shaw, R. J., "HSCT Research Picks up Speed," *Aerospace America*, Aug., 1997, pp. 24-29.
- [3] Takazawa, K. : "Promotion of Research on Next-Generation Supersonic Transport Technology with the Use of Unmanned Sub-Scaled Experimental Aircraft," *Proc. of Aircraft Symposium*, 1996, pp. 383-388.
- [4] Yoshida, T., Tsutsui, H., Takahashi, K. and Sanda T., "Application of Active Control Technologies and Structural Optimization for Supersonic Commercial Transport," *Proc. of World Aviation Congress*, Los Angeles, 1996, pp. 1-9.
- [5] Saitoh, K., Matsushita, H., Hashidate M. and Baldelli, D. H., "Active Flutter Suppression of a Flexible Wing in Transonic Region," *Proc. of Int. Forum on Aeroelasticity and Structural Dynamics*, 1994, pp. 581-586.
- [6] Baldelli, D. H., Ohta, H., Matsushita, H., Hashidate, M., and Saitoh, K., "Flutter Margin Augmentation Synthesis Using Normalized coprime Factors Approach," *J. Guidance, Control, and Dynamics*, Vol. 18, No. 4, 1995, pp. 802-811.
- [7] Saitoh, K., Baldelli, D. H., Matsushita, H. and Hashidate, M., "Robust Controller Design and Its Experimental Validation for Active Transonic Flutter Suppression," *Proc. of Int. Forum on Aeroelasticity and Structural Dynamics*, 1997, pp. 393-399.
- [8] Ueda, T. and Dowell, E. H., "A New Solution Method for Lifting Surfaces in Subsonic Flow," *AIAA Journal*, Vol. 20, 1982, pp. 348-355.
- [9] Zhou, K., *Robust and Optimal Control*, Prentice-Hall, 1996.
- [10] Fujimori, A. and Ohta, H., "A Synthesis of Reduced-Order H_∞ Controllers for Active Flutter Suppression Systems," *Proc. of 12th IFAC World Congress*, Vol.3, 1993, pp.805-808.